International Journal of Chronic Obstructive Pulmonary Disease Dovepress
open access to scientific and medical research

Open Access Full Text Article

ORIGINAL RESEARCH

Hypermethylation of the Nrf2 Promoter Induces Ferroptosis by Inhibiting the Nrf2-GPX4 Axis in COPD

Zixiao Zhang[1,*]
Congli Fu[1,2,*]
Jiaxin Liu[1]
Xiaoyan Sai[1]
Chu Qin[1]
Tingting Di[1]
Yue Yang[1]
Yan Wu[1]
Tao Bian[1]

[1]Department of Respiratory Medicine, Wuxi People's Hospital Affiliated to Nanjing, Medical University, Wuxi, Jiangsu, 214023, People's Republic of China; [2]Department of Pulmonary and Critical Care Medicine, Zhejiang Provincial People's Hospital, People's Hospital of Hangzhou Medical College, Hangzhou, Zhejiang, 310014, People's Republic of China

*These authors contributed equally to this work

Background: Nuclear factor E2-related factor 2 (Nrf2) is involved in oxidative stress and lung inflammation and regulates the etiology of chronic obstructive pulmonary disease (COPD). Ferroptosis is characterized by the accumulation of lipid reactive oxygen species (ROS) via ferrous ion-dependent Fenton reactions and is involved in COPD. However, the role of Nrf2 in ferroptosis and its epigenetic regulation in the pathogenesis of COPD remain unclear.

Methods: Ferroptosis was detected by 4-HNE, MDA, C11BODIPY, DCFH-DA, Peals' staining and CCK-8 assays. qPCR and Western blotting were performed to examine the Nrf2 levels in peripheral lung tissues, primary epithelial cells collected from patients with COPD and subjects with normal pulmonary function (never-smoker [control-NS]; smoker [control-S]), and cigarette smoke extract (CSE)-treated human bronchial epithelial (HBE) cells. ELISA was used to quantify IL-8 and IL-1β levels. Methylation of the Nrf2 promoter was analyzed by bisulfite sequencing and pyrosequencing.

Results: Ferroptosis was involved in COPD and glutathione peroxidase 4 (GPX4) expression was downregulated in the COPD group. Reactive oxygen species (ROS), lipid peroxides and MDA were increased, but GPX4 and SOD were exhausted in CSE-treated HBE cells. The production of IL-1β and IL-8 was promoted in HBE cells in response to CSE but could be reversed by the ferroptosis inhibitor fer-1. The Nrf2 level was significantly decreased in the COPD group compared with the control-S and control-NS groups. Increased Nrf2 expression enhanced GPX4 and SOD levels and inhibited ferroptosis and proinflammatory cytokines in the supernatant. Inhibition of GPX4 reversed the effect of Nrf2 overexpression and promoted ferroptosis. Two specific CpG sites within the Nrf2 promoter were hypermethylated in the COPD group. Similarly, CSE-treated HBE cells exhibited hypermethylation of the Nrf2 gene.

Conclusion: Nrf2 expression was downregulated in the lungs of COPD patients due to hypermethylation of the Nrf2 promoter, inhibiting Nrf2/GPX4 and ferroptosis, which is related to the initiation and progression of COPD. Targeting Nrf2/GPX4 may inhibit ferroptosis, which could provide strategies to delay or treat COPD.

Keywords: COPD, Nrf2, ferroptosis, GPX4, DNA methylation, oxidative stress, inflammation

Background

Chronic obstructive pulmonary disease (COPD) is a prevalent disease that seriously endangers people's health. COPD has been projected to become the third leading cause of death in the world by 2030.[1] It is characterized by high morbidity and mortality, leading to substantial socioeconomic burdens.[2] Permanent destruction of terminal bronchioles is a pathological characteristic of COPD and is associated with

Correspondence: Tao Bian; Yan Wu
Department of Respiratory Medicine, Wuxi People's Hospital Affiliated to Nanjing Medical University, Wuxi, Jiangsu, 214023, People's Republic of China
Email btaophd@sina.com; wuyanyangting@163.com

Received: 23 September 2021
Accepted: 22 November 2021
Published: 14 December 2021

amplified oxidative stress and inflammatory responses.[3–5] High exposure to harmful particles or gases such as cigarette smoke (CS) has been determined to be the primary causal mechanism for this amplified inflammation and oxidative stress.[6–8] Long-term exposure to CS leads to the accumulation of reactive oxygen species (ROS) in airway epithelial cells, followed by plasma membrane damage and the release of damage-associated molecular patterns (DAMPs), which in turn trigger inflammation and active cell death pathways.[9,10] Although many types of cells and mediators are involved in the pathophysiological process of COPD,[11] data from the literature have indicated the key role of Nrf2, which is strongly upregulated by oxidants.[2]

Nrf2 is a critical factor in maintaining the oxidation/antioxidant balance.[12,13] Under stress conditions, Nrf2 dissociates from Kelch-like ECH-associated protein 1 (Keap1) and then translocates into the nucleus, binding to the antioxidant response element (ARE) to initiate the transcription of downstream genes,[14,15] such as glutathione peroxidase (GPX), heme oxygenase-1 (HO-1), and NAD(P)H quinone oxidoreductase, which are known to protect against oxidative damage.[13,16,17] Moreover, Nrf2 expression was highly elevated in mild COPD patients but significantly decreased in patients with GOLD stage III and IV COPD.[18–20] Nrf2-deficient mice appeared to develop emphysema earlier after exposure to CS.[21] Therefore, dysregulation of oxidative stress and inflammation could contribute to the pathogenesis of COPD. The potential role of Nrf2 in oxidative stress and inflammation in COPD therapy is expected to be further elucidated.

Ferroptosis is a form of iron-dependent oxidative cell death characterized by the overwhelming accumulation of lipid ROS during Fenton reactions and the release of DAMPs.[22,23] An imbalance between mitochondria and the NADPH oxidase-mediated oxidative stress system or the GSH-, CoQ10- and BH_4-mediated antioxidant system promotes ferroptosis.[13] Disrupted iron homeostasis also results in excessive oxidative stress and ferroptosis.[24] Nrf2 plays a major role in regulating the expression of antioxidants or iron metabolism genes, which regulate iron/metal metabolism, intermediate metabolism, and GSH synthesis/metabolism and contribute to ferroptosis.[25–27] As a result, activating Nrf2 alleviates lipid peroxidation and ferroptosis in intestinal ischemia, tumors, acute lung injury and other diseases.[17,25] Glutathione peroxidase 4 (GPX4) deficiency and NCOA4-mediated selective autophagic turnover of ferritin (ferritinophagy) initiate the progression of ferroptosis in COPD.[24] Disruption of ferroptosis via antioxidant pathways may be a potential method for COPD treatment; however, the mechanism by which Nrf2 participates in ferroptosis in COPD has not been elucidated.

The purpose of this study was to confirm the pivotal role of Nrf2 in the regulation of ferroptosis in COPD and to identify the epigenetic mechanisms involved in its regulation. Here, we investigated the expression and epigenetic regulation of Nrf2 and the mechanism by which the Nrf2 signaling pathway in ferroptosis is related to COPD. These findings elucidated the pathways of ferroptosis in bronchial epithelial cells in COPD and revealed Nrf2 as a potential target for COPD treatment.

Methods

Subjects

All volunteers were recruited from Wuxi People's Hospital Affiliated to Nanjing Medical University and included nonsmokers without COPD (Control-NS), smokers without COPD (Control-S) and COPD subjects. COPD patients were diagnosed based on the Global Initiative for Chronic Obstructive Lung Disease (GOLD) clinical criteria for the diagnosis and classification of COPD. Lung tissues were collected from COPD patients scheduled for lung transplantation or pulmonary lobectomy for small nodules in Wuxi People's Hospital. Lung tissues were transferred into liquid nitrogen and stored at −80 °C. Primary bronchial epithelial cells were collected from patients with or without COPD scheduled for bronchoscopies for small nodules or a small amount of bloody sputum in Wuxi People's Hospital.

The lung function and basic information of the subjects participating in the study are shown in Tables 1 and 2.

All experimental work with humans was approved by the Ethics Committee of the Wuxi People's Hospital Affiliated to Nanjing Medical University. This study was conducted in accordance with the Declaration of Helsinki. All subjects provided written informed consent.

Reagents and Cell Culture

Study subjects were patients with or without COPD scheduled for bronchoscopies for small nodules or a small amount of bloody sputum at Wuxi People's Hospital. After using 20 mL of normal saline to lavage the second- and third-generation bronchi, 5 consecutive

Table 1 Clinical Characteristics of the Enrolled Subjects from Whom Bronchial Epithelial Cells Were Collected

	Nonsmokers Without COPD (Control-NS) (n=8)	Smokers Without COPD (Control-S) (n=9)	Patients with COPD (n=16)	Between-Group Differences (p value)
Age, y	56.50±8.144	61.56±3.930	66.11±2.019	0.432
Sex ratio (F/M)	0/8	0/9	0/16	1.000
Pack-years	0±0	39.38±8.042	47.03±8.860	0.0014
FEV1/FVC	88.63±6.57	83.73±4.28	57.45±9.31	0.000
FEV1% pred	105.5±10.07	88.70±5.33	55.14±13.40	0.000

Note: Values are presented as the means ± SD.
Abbreviations: COPD, chronic obstructive pulmonary disease; pack-year, number of cigarettes smoked per day/20 (pack) × duration of smoking (year); FEV1, forced expiratory volume in one second; FVC, forced vital capacity; FEV1% pred, forced expiratory volume in one second per cent predicted.

Table 2 Clinical Characteristics of Enrolled Subjects from Whom Lung Tissues Were Collected

	Nonsmokers Without COPD (Control-NS) (n=11)	Smokers Without COPD (Control-S) (n=7)	Patients with COPD (n=8)	Between-Group Differences (p value)
Age, y	58.36±4.048	63.14±1.550	59.38±1.362	0.5045
Sex ratio (F/M)	7/4	1/6	1/7	0.5045
Pack-year	0±0	25±6.583	8.750±5.154	0.0004
FEV1/FVC (%)	88.2±6.63	82.06±3.89	37.48±8.37	0.000
FEV1% pred	102.79±14.29	91.91±6.10	33.89±12.38	0.000

Note: Values are presented as the means ± SD.
Abbreviations: COPD, chronic obstructive pulmonary disease; pack-year, number of cigarettes smoked per day/20 (pack) × duration of smoking (year); FEV1, forced expiratory volume in one second; FVC, forced vital capacity; FEV1% pred, forced expiratory volume in one second per cent predicted.

brushings (Anrei, China) were sampled from the bronchial mucosa. After each brush, cells were harvested into a tube containing 5 mL of RPMI 1640 (Gibco, USA) with 1% penicillin-streptomycin (P/S). Approximately 25 mL of liquid was filtered through a cell strainer (Falcon, USA). After 5 min of centrifugation at 3000 rpm, the cell pellets were washed twice with 2 mL of RPMI 1640, and the final cell pellets were resuspended in BEGM (Lonza, USA). Primary human bronchial epithelial cells were harvested after 7 to 25 days of culture.

HBE cells (ATCC, USA) were maintained in DMEM (Gibco, USA) containing 10% FBS and 1X P/S under 5% CO_2 at 37 °C. When HBE cells reached a confluence of approximately 5×10^5 per well, the medium was replaced with serum-free high-glucose DMEM for 24 h. Nrf2-overexpressing HBE cells were obtained by transfection with an NFE2L2 overexpression (OE) lentiviral vector. HBE cells were treated with 10 μM fer-1 (Sigma-Aldrich, USA) and 1 μM RSL3 (Sigma-Aldrich) for 1 h before they were exposed to 5% CS extract (CSE) for 72 h.

Establishment of a Murine COPD Model

Male C57BL6 mice at 6–8 weeks of age were purchased from Changzhou Cavans Animal Experiment Co., Ltd., and housed in animal facilities at Wuxi People's Hospital. Mice were exposed to CS from cigarettes (Daqianmen, China) in a whole-body exposure system for 4 h a day for 24 weeks.[28] Age-matched mice kept in a similar environment without exposure to CS served as controls. Mouse lung function was measured using whole-body plethysmography (Buxco Electronics, Ltd., USA). Enhanced pause (Penh) was chosen as the parameter to indicate restricted airflow and was calculated as previously described: Penh = (Te/Tr – 1) × (PEF/PIF) (Te: the expiration time, Tr: relaxation time, PIF: peak inspiratory flow, PEF: peak expiratory flow).[28] The procedures for the care and use of animals were approved by the Ethics Committee of Nanjing Medical University (KY21023). The animals used in this study were maintained in accordance with the ethical guidelines of the Guiding Principles in the Care and Use of Animals (China) and the Policy of Animal Care and Use Committee of Nanjing Medical University. Humane care was provided according to the 3R principles of animal experiments.

Preparation of CSE

A cigarette contains 10 mg tar and 0.8 mg nicotine (Daqianmen, China). The smoke of two cigarettes was

bubbled into 10 mL of high-glucose DMEM (Gibco, USA). The CSE was sterilized by filtering the solution through a 0.22-μm filter (Millipore, Germany) and adjusted to pH 7.4. The solution was standardized by monitoring the absorbance at 320 and 540 nm. The CSE was regarded as 100% and was subsequently diluted with high-glucose DMEM.

Transmission Electron Microscopy (TEM)

HBE cells were treated with trypsin-EDTA (Gibco, USA) and centrifuged at 3000 rpm for 10 min. After the supernatant was removed, cell pellets were fixed in 5% glutaraldehyde at 4 °C overnight. Fixed HBE cells were then embedded in epoxy resin and sliced into ultrathin sections, which were stained with uranyl acetate and lead citrate. Images viewed under a transmission electron microscope were obtained.

Immunohistochemistry (IHC)

Lung tissues were fixed in 4% paraformaldehyde solution (Beyotime, China) for 24 h and then dehydrated and embedded in paraffin following routine methods. The slides were rinsed with Bond Dewax Solution at 72 °C to deparaffinize the tissue slices. Then, the sections were treated with Enhanced Endogenous Peroxidase Blocking Buffer (Beyotime) for 5 min to block endogenous peroxidase activity before they were incubated with Nrf2 antibody (1:500 dilution, Abcam, USA), 4-HNE antibody (1:200 dilution, Abcam) or GPX4 antibody (1:500 dilution, Abcam) overnight, after which DAB was quickly added. The color rendering time was controlled for 5 min. Images viewed under an Olympus microscope were captured. The Nrf2 immunostaining results were scored by multiplying the percentage of positive cells (0, <10%; 1+, 10–25%; 2+, 25–50%; 3+, 50–75% or 4+, >75%) by the staining intensity (0, negative; 1+, weak; 2+, moderate; or 3+, strong), and the 4-HNE and GXP4 immunostaining results were scored as the integrated optical density (IOD)/area as detected by Image-Pro Plus.

Hematoxylin-Eosin (H&E) Staining and Morphological Analysis

Mouse lung tissue was fixed in 4% paraformaldehyde solution, sliced, and stained with hematoxylin for 5 min. The slides were washed with PBS, differentiated with hydrochloric acid-ethanol for 3 sec, stained with eosin for 2 min, and mounted with neutral resin. Finally, pathological changes in the mouse lung tissue were observed under an Olympus microscope. The size of the alveolar space was examined by measuring the mean linear intercept (MLI) and mean alveolar number (MAN) as previously described.[28] The MLI was measured by dividing the length of a line drawn across the lung section by the total number of intercepts counted within this line at 100× magnification.[29] The MAN was measured by dividing the area into the count of alveolar numbers at 100× magnification.

Immunofluorescence (IF)

Cells were fixed with 4% paraformaldehyde for 30 min and washed with PBS 3 times after they were permeabilized with 0.3% Triton X-100 (Beyotime) for 10 min. The cells were then blocked with PBS containing 5% goat serum for 1 h and incubated with the primary antibody (1:200; Abcam) overnight at 4 °C. The cells were then incubated with the fluorescent-conjugated secondary antibody at room temperature for 1 h, and DAPI was added for 5 min. Images viewed under a fluorescence microscope were obtained.

RNA Isolation and Reverse Transcription PCR

RNA was isolated from tissues and cells by using RNAiso Plus (TaKaRa, Japan). cDNA synthesis was performed using a reverse transcription kit (TaKaRa, Japan), and the synthesized DNA was stored at −20 °C. qPCR analysis was performed with TB Green™ Premix Ex Taq™ II (TaKaRa, Japan). Steps were performed according to the manufacturer's protocol. All data were normalized to the expression of GAPDH mRNA. The primer sequences were as follows: GAPDH (forward 5′- CCTTCCGTGTCCCCACT −3′, reverse 5′- GCCTGCTTCACCACCTTC −3′), Nrf2 (forward 5′- GGTTGCCCACATTCCCAAA −3′, reverse 5′- AGTGACTGAAACGTAGCCGA −3′), and GPX4 (forward 5′- ATGGTTAACCTGGACAAGTACC −3′, reverse 5′ - GACGAGCTGAGTGTAGTTTACT −3′).

Protein Lysis and Western Blotting

Total protein was extracted from cells using RIPA buffer (KeyGEN, China), followed by centrifugation at 14,000 ×g for 10 min. Equal amounts of protein (20 μg) were separated via SDS-PAGE through 10% gels and transferred onto PVDF membranes (Immobilon-P membrane, Millipore). After 1 h of blocking in 5% milk, the membranes were incubated with

antibodies targeting Nrf2 (Abcam), GPX4 (Abcam) or β-actin (Proteintech, China) at 4 °C overnight. After incubation with horseradish peroxidase (HRP)-conjugated secondary antibody (Jackson ImmunoResearch, USA) for 1 h, protein bands were developed in an automatic exposure machine (ProteinSimple, USA).

The ROS Measurement

HBE cells were incubated with 10 μM DCFH-DA (Sigma-Aldrich, USA) at 37 °C for 30 min. The supernatant was removed, and the cells were washed with DMEM without FBS twice. Images viewed under a fluorescence microscope were obtained.

Measurement of Lipid Peroxidation

HBE cells were sonicated with cell lysis buffer (Beyotime) and then centrifuged at 12,000 ×g for 10 min at 4 °C. The supernatant was collected for the MDA assay (Beyotime) following the manufacturer's protocol. MDA levels were detected at a wavelength of 532 nm.

For the C11BODIPY probe (Invitrogen, USA), HBE cells were incubated with 1 μM C11BODIPY at 37 °C for 30 min in DMEM and then washed with PBS 3 times. The red and green fluorescence signals in the cells were viewed under a fluorescence microscope.

Superoxide Dismutase Assay

The relative superoxide dismutase (SOD) concentration in cell lysates was assessed using a superoxide dismutase (SOD) assay kit (Nanjing Jiancheng Bioengineering Institute, China) according to the manufacturer's instructions.

CCK-8 Assay

A CCK-8 assay was performed to detect cell viability according to the manufacturer's protocol (Beyotime). Approximately 5×10^3 cells were seeded in 96-well plates. The cells were treated with 10 μL of CCK-8 solution for 24, 48, and 72 h and incubated in the dark for another 2 h. The absorbance was measured at a wavelength of 450 nm.

Perls' DAB Staining

Perls' DAB staining was performed as previously described to detect the presence of ferric iron in tissue.[24] Paraffin-embedded lung sections were incubated in freely prepared Perls' solution (Sigma-Aldrich, USA) for 1 h and then incubated with DAB for 1 min. Images viewed under an Olympus microscope were obtained.

Bisulfite Sequencing Analysis

Total DNA was extracted using a QIAamp DNA Mini Kit (51304, Qiagen) following the manufacturer's instructions. Bisulfite conversion was performed using 500 ng of genomic DNA with an EpiTect® Bisulfite kit (59104, Qiagen), and the DNA was purified.[30] Each sample contained plasmid DNA from at least 10 colonies and was prepared using a BiQ-Analyzer before sequencing.

Pyrosequencing Analysis

Two CpG sites were selected based on the results of the bisulfite sequencing analysis. Bisulfite-converted DNA was amplified by PCR with the reactions and conditions described in the PyroMark PCR kit. Pyrosequencing was performed using the PyroMark Gold Q96 pyrosequencer (Qiagen) according to the manufacturer's instructions, and the percentage methylation per CpG was then calculated.

ELISA

After HBE cells were treated with CSE, the supernatants were collected, and IL-8 (R&D Systems, USA) and IL-1β (Absin, China) levels were detected by ELISA. The absorbance was measured at a wavelength of 450 nm.

Statistical Analysis

All experiments were performed in at least three independent assays and are presented as the mean ± standard error of the mean (S.E.M.). Comparisons between two different groups were performed using the two-tailed Student's *t*-test. One-way ANOVA was used for comparisons between more than two groups, and Tukey post hoc tests were performed to test for statistical significance. P-values of less than 0.05 were considered statistically significant.

Results

Ferroptosis is Involved in Human and Murine COPD Lung Tissues

The lung function and basic information of the subjects participating in the study are shown in Tables 1 and 2. To elucidate the involvement of ferroptosis in COPD, we evaluated 4-HNE and nonheme iron levels by IHC and Perls' staining. IHC of COPD lung tissue showed increased expression of 4-HNE (Figure 1A and B). Perls' DAB staining indicated increased Fe^{3+} in the bronchial epithelial cells of the lung tissue of COPD patients and smokers (Figure 1C). These results suggest enhanced deposition of nonheme iron and aldehyde products of

phospholipid peroxidation in bronchial epithelial cells, indicating that ferroptosis participates in COPD pathogenesis.

We established a COPD mouse model as described in the Materials and Methods section. In CS-exposed mice, the alveolar space was enlarged according to H&E staining (Figure 1D). The MLI (Figure 1E) and MAN (Figure 1F) indicated enhanced airspace compared with that in the control mice. Penh is an important parameter that reflects airflow limitation. Compared with air-exposed mice, CS-exposed mice had an increased Penh (Figure 1G). The results above demonstrated that the murine model of COPD was successfully established, with enlarged alveolar space and limited airflow. In addition, we performed IHC and observed increased 4-HNE levels in CS-exposed mice (Figure 1H and I). Fe^{3+} was deposited in airway epithelial cells in lung tissue from CS-exposed mice (Figure 1J), whereas the lung tissue of control mice

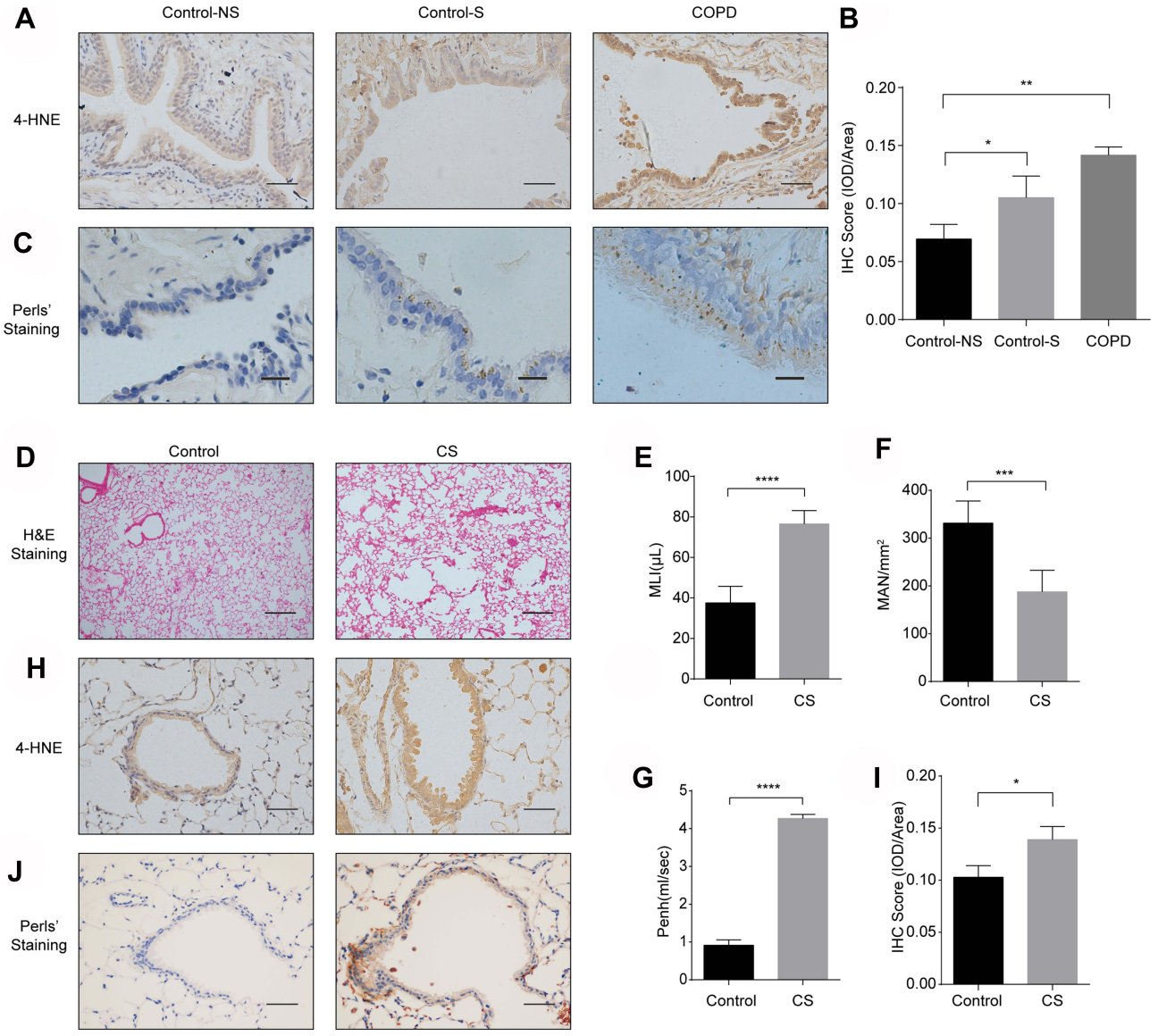

Figure 1 Ferroptosis is involved in human and murine COPD lung tissues. (**A**) Immunohistochemical (IHC) staining of 4-HNE in lung tissues from healthy volunteers (Control-NS), healthy smokers without COPD (Control-S) and COPD patients (original magnification ×400). Bar: 50 μm. The results were scored by (**B**) the integrated optical density (IOD)/area. (**C**) Fe^{3+} deposits were stained with Perls' DAB in lung tissues from Control-NS, Control-S and COPD patients (original magnification ×400). Bar: 20 μm. (**D–I**) C57BL6 mice were exposed to room air (Control) or cigarette smoke (CS) for 6 months. (**D**) H&E staining in lung sections of mice in the control and CS groups (original magnification ×100). Bar: 200 μm. At least 3 areas in tissues collected from each mouse were captured, and 3 mice in each group were analyzed. (**E** and **F**) The alveolar size was measured by the mean linear intercept (MLI) and mean alveolar number (MAN) at ×100 magnification. (**G**) Enhanced pause (Penh) of room air- and CS-exposed mice. (**H**) IHC staining of 4-HNE from lung sections of room air- and CS-exposed mice (original magnification ×400). Bar: 50 μm. The results were scored by (**I**) the IOD/area. (**J**) Fe^{3+} deposits were stained with Perls' DAB in air-exposed mice and CS-exposed mouse lungs (original magnification ×400). The results are presented as the means ± S.E.M. for three independent experiments. *P<0.05; **P < 0.01; ***P < 0.001; ****P < 0.0001.

showed little Fe^{3+} deposition, indicating increased ferroptosis in CS-exposed mice.

CSE Induced Ferroptosis and the Release of IL-1β and IL-8 in HBE Cells

Using TEM, we observed that HBE cells treated with CSE exhibited the characteristic morphological features associated with ferroptosis, such as mitochondria with vestigial cristae (Figure 2A).[22,31] We also determined the characteristic morphological features associated with ferroptosis in CSE-exposed A549 cells (Supplementary Figure 1A). ROS can react with the polyunsaturated fatty acids of lipid membranes and induce lipid peroxidation. SOD plays an important role in antioxidant activity and prevent ROS-initiated reactions.[32] To elucidate the involvement of ferroptosis in CSE-treated HBE cells, we evaluated CS-induced ROS accumulation detected by DCFH-DA (Figure 2B) and lipid peroxidation detected by C11BODIPY (Figure 2C) and MDA (Figure 2D). ROS were increased and SOD (Figure 2E) were decreased in response to CSE. CSE-treated HBE cells exhibited enhanced lipid peroxidation compared with the control cells and lower cell viability based on the CCK-8 results (Figure 2F). The increased ROS and lipid peroxidation and decreased SOD and cell viability could be reversed by treatment with fer-1, a ferroptosis inhibitor that scavenges the initiating alkoxyl radicals produced, together with other rearrangement products, by ferrous iron from lipid hydroperoxides (Figure 2B–F).[33] We also observed increased lipid peroxidation in A549 cells in response to CSE (Supplementary Figure 1B). Ferroptosis has been shown to play an important role in inflammation and

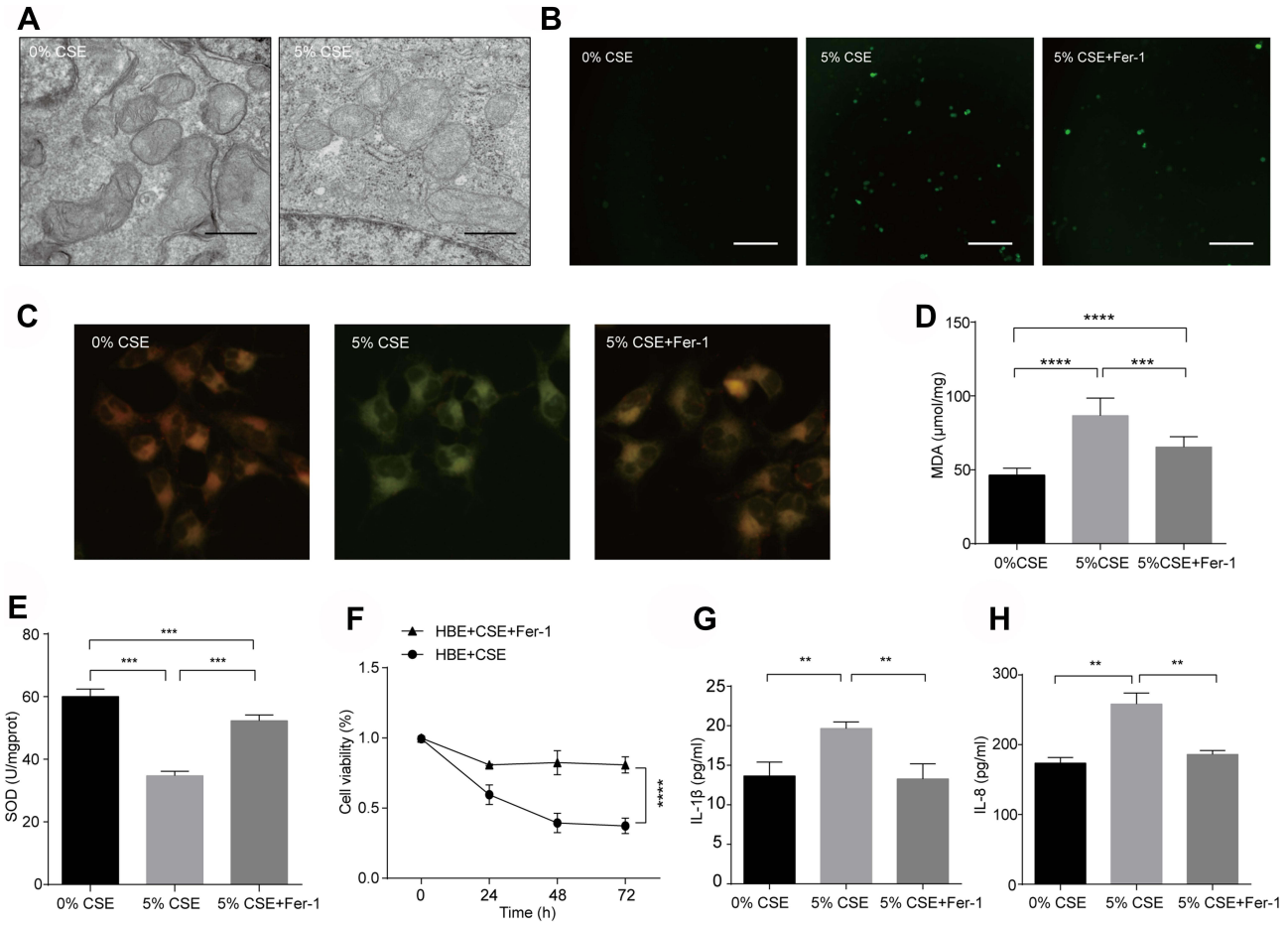

Figure 2 CSE induced ferroptosis and the release of IL-1β and IL-8 in HBE cells. (**A**) Representative TEM images of mitochondria in HBE cells treated with 0% or 5% CSE for 72 h. Bar: 500 nm. (**B–F**) HBE cells were treated with 0% or 5% CSE for 72 h. Fer-1 (10 μmol/L) was added to DMEM 1 h before CSE exposure. (**B**) Images of intracellular ROS stained by DCFH-DA were captured with a fluorescence microscope. Original magnification ×100. Bar: 200μm. (**C**) Representative images of C11BODIPY in the green and red channels in each group were captured with a fluorescence microscope. Upon oxidation in live cells, fluorescence shifts from red to green. An overlay of the green and red channels is shown. Original magnification ×400. (**D**) The MDA and (**E**) SOD levels in each group are shown. (**F**) Cell viability was detected by the CCK-8 assay and all values were normalized to those of the 0% CSE group. (**G**) ELISA of IL-1β and (**H**) IL-8 in the supernatant of HBE cells is shown. The results are shown as the mean ± S.E.M. for three independent experiments. **P < 0.01; ***P < 0.001; ****P < 0.0001.

induces the release of DAMPs and other proinflammatory cytokines, such as TNF, PGE2, IL-1β, IL-6 and IL-8.[34] To determine the proinflammatory role of ferroptosis in COPD, we performed ELISA to detect the levels of IL-8 and IL-1β in the supernatant of HBE cells. CSE exposure increased the levels of IL-8 and IL-1β. Similarly, fer-1 decreased the production of IL-1β (Figure 2G) and IL-8 (Figure 2H). The results above demonstrated the presence of ferroptosis in CSE-exposed HBE cells and the proinflammatory role of ferroptosis.

GPX4 is Downregulated in the Lungs of COPD Patients, Murine Models and CSE-Treated HBE Cells

GPX4 is an essential regulator of ferroptosis that functions by suppressing lipid peroxidation generation.[35] To demonstrate the mechanism of ferroptosis in COPD, GPX4 levels were assessed by IHC and Western blot analysis. IHC of COPD lung tissue showed downregulation of GPX4 expression in bronchial epithelial cells (Figure 3A and B). Western blot analysis demonstrated a reduction in GPX4 expression in COPD lung tissue (Figure 3C and D). However, there were no significant differences in GPX4 levels in nonsmokers and smokers without COPD. We isolated primary human bronchial epithelial cells via bronchoscopy brush examination and examined the expression of GPX4 in different subjects. In contrast to cells from volunteers and healthy smokers, COPD primary bronchial epithelial cells showed reduced GPX4 expression (Figure 3E and F). Consistent with the downregulated levels of GPX4 in COPD lung tissue and primary human bronchial epithelial cells, GPX4 expression was decreased in bronchial epithelial cells of CS-exposed mice, as detected by IHC (Figure 3G and H) and Western blots (Figure 3I and J). Downregulation of GPX4 was also observed in alveolar type II epithelial cells in the CS-exposed mice, as detected by IHC (Supplementary Figure 2A and B). GPX4 expression was significantly reduced in response to CSE exposure for 72 h in HBE cells (Figure 3K and L). GPX4 was decreased in A549 cells upon CSE exposure as well (Supplementary Figure 1C and D). The results above indicate the downregulation of GPX4 expression in COPD tissues in vivo and CSE-exposed HBE cells in vitro. In addition, epithelial cells are critical with respect to the effects of reduced GPX4 expression on COPD.

Nrf2 is Reduced in the Lungs of COPD Patients, Murine Models and CSE-Treated HBE Cells

Using IHC staining methods, we found that positive staining of Nrf2 was primarily located in epithelial cells in the lung tissues of COPD patients (Figure 4A and B). COPD patients showed decreased protein (Figure 4C and D) and mRNA levels of Nrf2 (Figure 4E). As shown in Figure 4G and H, Nrf2 was minimally observed in COPD primary epithelial cells but was strongly expressed in normal cells. The mRNA levels of Nrf2 in COPD primary epithelial cells were also decreased (Figure 4I). Nrf2 was primarily expressed within epithelial cells and was mainly located in the cytoplasm (Figure 4F). We also observed that Nrf2 was decreased in 6-month CS-exposed mice (Figure 4J and K) and CSE-exposed HBE cells in vitro (Figure 4L and M). The reductions in Nrf2 protein expression in peripheral lung tissues and primary epithelial cells of COPD patients, murine models and CSE-treated HBE cells suggest that epithelial cells are important with respect to the effects of reduced Nrf2 expression in COPD.

The Nrf2-GPX4 Axis Mitigates CSE-Induced Ferroptosis and the Release of IL-1β and IL-8 in HBE Cells

It has been reported that Nrf2 can induce the transcription of GPX4.[27] To determine whether Nrf2 could alleviate ferroptosis in CSE-treated HBE cells, a lentivirus vector was used to promote Nrf2 overexpression. The protein (Figure 5A and C) and mRNA (Figure 5E) levels of GPX4 were elevated in response to stress conditions when Nrf2 was overexpressed (Figure 5A, B and D). Overexpression of Nrf2 decreased ROS production (Figure 5F) and restored SOD (Figure 5I). The high lipid peroxidation (Figure 5G and H) and low cell viability (Figure 5J) caused by CSE were alleviated in cells ectopically expressing Nrf2. RSL3, a drug that binds to and inactivates GXP4, was shown to reverse the effect of Nrf2 overexpression and promote ferroptosis (Figure 5F–J). Activation of Nrf2-GPX4 reduced the secretion of IL-1β (Figure 5K) and IL-8 (Figure 5L). However, IL-1β and IL-8 levels were enhanced upon RSL3 treatment. The results above suggest that the Nrf2/GPX4 axis mitigates ferroptosis and further inhibits inflammation in CSE-treated HBE cells.

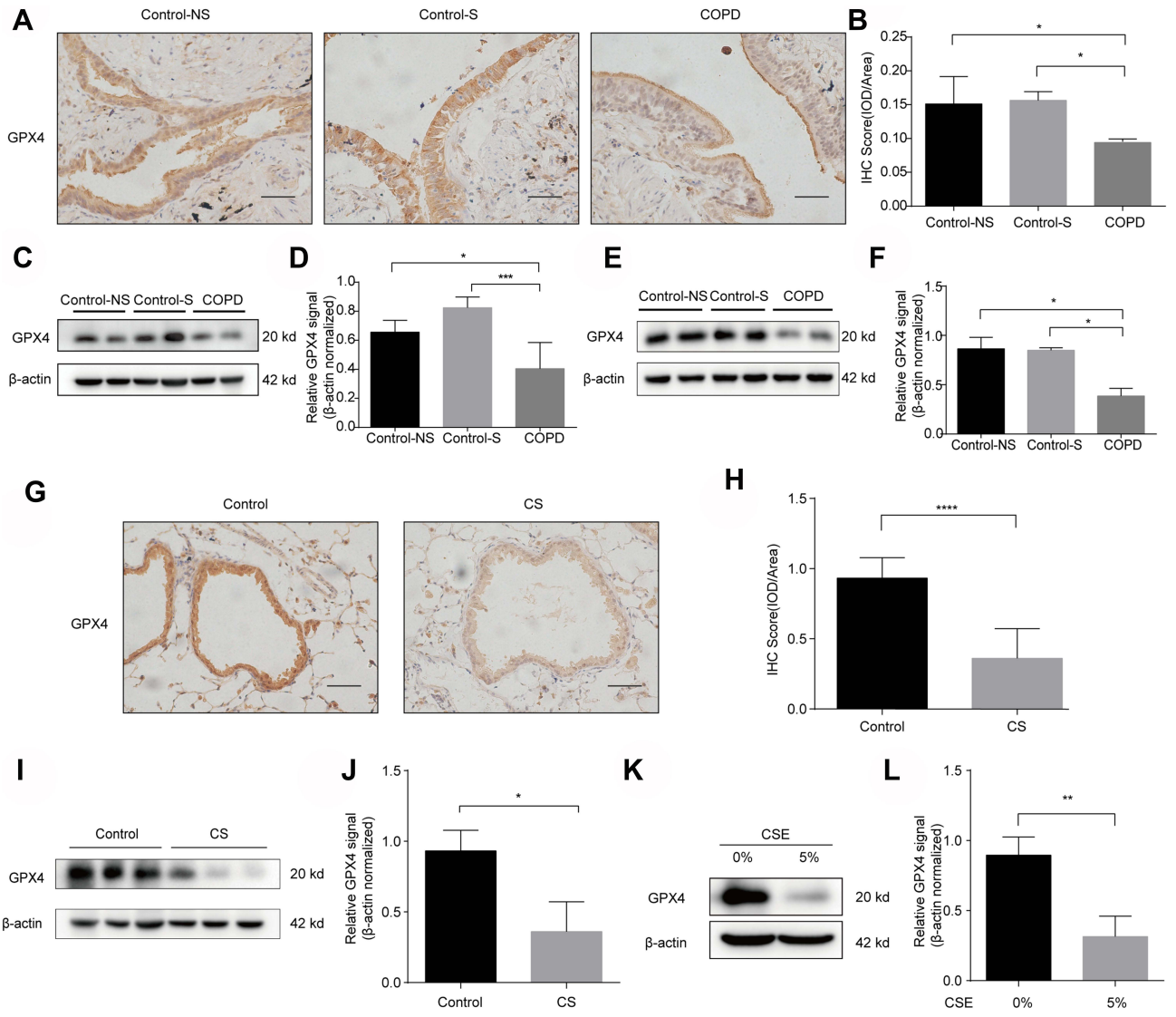

Figure 3 GPX4 expression is downregulated in the lungs of COPD patients, murine models and CSE-treated HBE cells. (**A**) GPX4 immunostaining of lungs from Control-NS, Control-S and COPD patients is shown (original magnification ×400). Bar: 50 μm. The results were scored by (**B**) IOD/area. (**C**and**D**) Western blots of human lung homogenates from Control-NS, Control-S and COPD patients were probed using an anti-GPX4 antibody and normalized to β-actin levels (loading control). (**E** and **F**) Western blots of primary bronchial epithelial cells from Control-NS, Control-S and COPD patients were probed using an anti-GPX4 antibody and normalized to β-actin (loading control). (**G–J**) C57BL6 mice were exposed to room air (Control) or cigarette smoke (CS) for 6 months. (**G** and **H**) IHC staining of GPX4 in lungs from room air (Control)- and CS-exposed mice. Original magnification ×400. Bar: 50 μm. The results were scored by (**H**) IOD/area. (**I** and **J**) The expression levels of GPX4 in lung homogenates of room air (Control)- and CS-exposed mice were measured by Western blot analysis and normalized to those of β-actin. (**K** and **L**) The protein level of GPX4 in HBE cells treated with 0% or 5% CSE for 72 h was measured by Western blot and normalized to β-actin levels (loading control). The results are presented as the means ± S.E.M. from three independent experiments. *P<0.05; **P < 0.01; ***P < 0.001, ****P < 0.0001.

Specific CpG Sites in the Nrf2 Promoter are Hypermethylated in Human COPD Lung and CSE-Treated HBE Cells

We identified the human Nrf2 genome sequence (NC_000002) by sequence analysis and found CpG islands in the human Nrf2 promoter region. To identify whether aberrant DNA methylation could be associated with Nrf2 expression in COPD patients, we analyzed the methylation levels of CpG sites in the Nrf2 promoter (−632 to −1) in peripheral lung tissues by bisulfite sequencing. We found that the first site (−632 bp, 6.7% ±3.3% in Control-NS, 10%±0% in Control-S and 30%±10% in COPD) and second site (−580 bp, 0%±0% in Control-NS, 0% ±0% in Control-S and 13.6%±3.3% in COPD) were hypermethylated in peripheral lung tissues of COPD patients compared with control subjects (Figure 6A and B). Bisulfite sequencing was performed to filter out significant CpG sites within the Nrf2 promoter. To assess the exact degree of methylation at these sites, we conducted pyrosequencing analysis

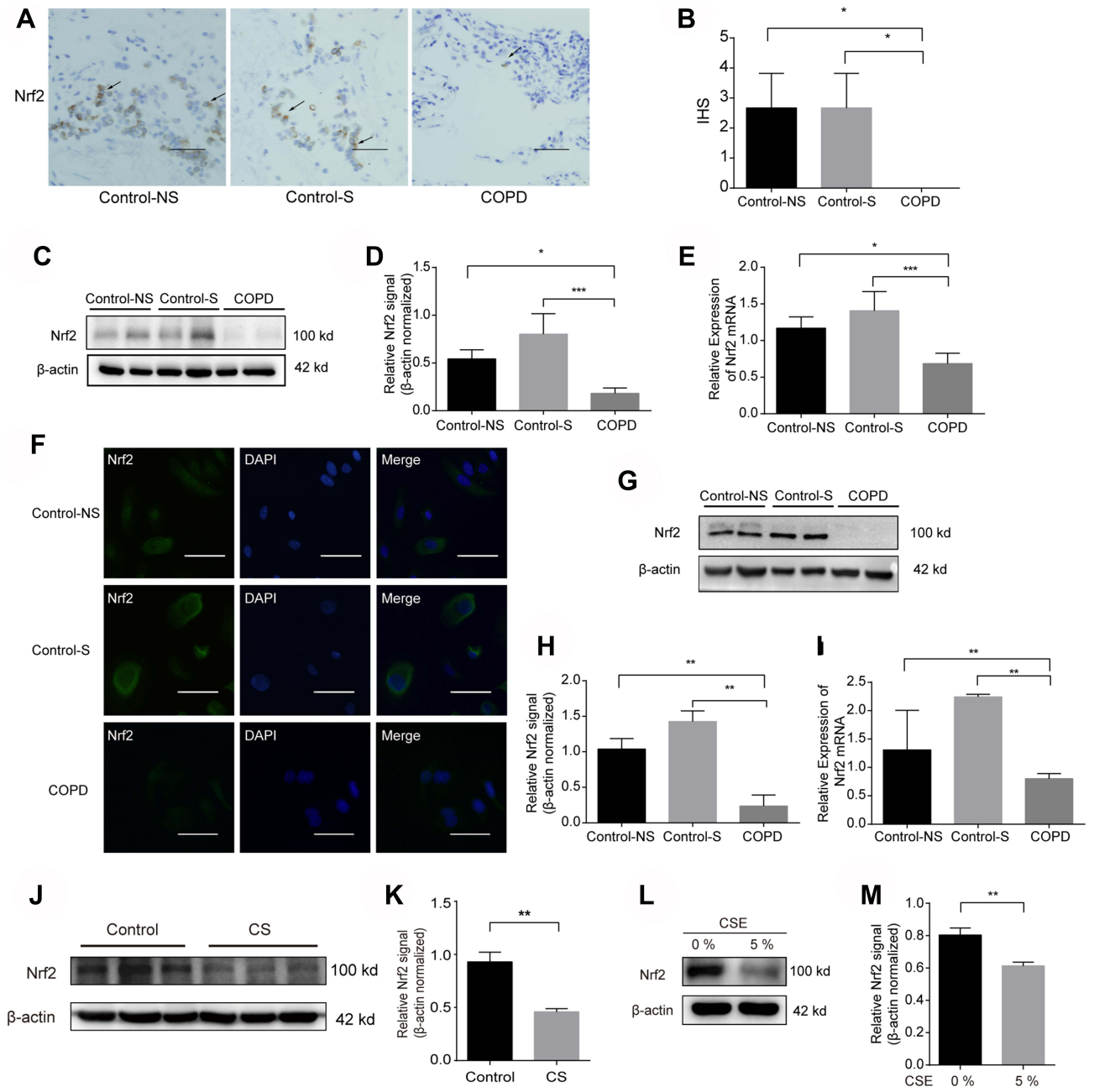

Figure 4 Nrf2 is reduced in the lungs of COPD patients, murine models and CSE-treated HBE cells. (**A**) Nrf2 immunostaining was markedly reduced in COPD patients compared with that in Control-NS and Control-S. The arrows represent airway epithelial cells. Original magnification ×100. Bar: 200 μm. (**B**) The immunostaining score in airway epithelial cells (average ± S.E.M.) obtained from 10 image fields (200X) for each sample is shown in the right panel. (**C** and **D**) Western blots of human lung homogenates from Control-NS, Control-S and COPD patients were probed using an anti-Nrf2 antibody and normalized to β-actin (loading control). (**E**) The mRNA level of Nrf2 in lung tissues from Control-NS, Control-S and COPD patients was measured by real-time RT-PCR. The data presented are the relative mRNA levels normalized to GAPDH levels. (**F**) Immunofluorescence images of primary bronchial epithelial cells from Control-NS, Control-S and COPD patients. The green fluorescence in the panels on the left-hand side indicates Nrf2, the blue stain indicates the nucleus, and the merged panels are on the right. Original magnification ×400. Bar: 50μm. (**G** and **H**) The protein levels of Nrf2 in primary bronchial epithelial cells derived from patients were measured by Western blot and normalized to β-actin. (**I**) mRNA levels of Nrf2 in primary bronchial epithelial cells derived from patients were measured by RT-PCR. The data presented are the relative mRNA levels normalized to GAPDH levels. (**J** and **K**) The protein level of Nrf2 in the lung homogenate of room air (Control) and CS-exposed mice after 6 months was measured by Western blots and normalized to β-actin (loading control). (**L** and **M**) The protein level of Nrf2 in CSE-exposed HBE cells for 72 h was measured by Western blots and normalized to β-actin (loading control). The results are the means ± S.E.M. for three independent experiments. *P<0.05; **P < 0.01; ***P < 0.001.

with lung tissues, primary epithelial cells and HBE cells treated with 5% CSE. We found that the first two sites were methylated in lung tissues from COPD patients (Figure 6C and D), while only the first site was methylated in primary epithelial cells (Figure 6E and F) and CSE-treated HBE cells (Figure 6G and H).

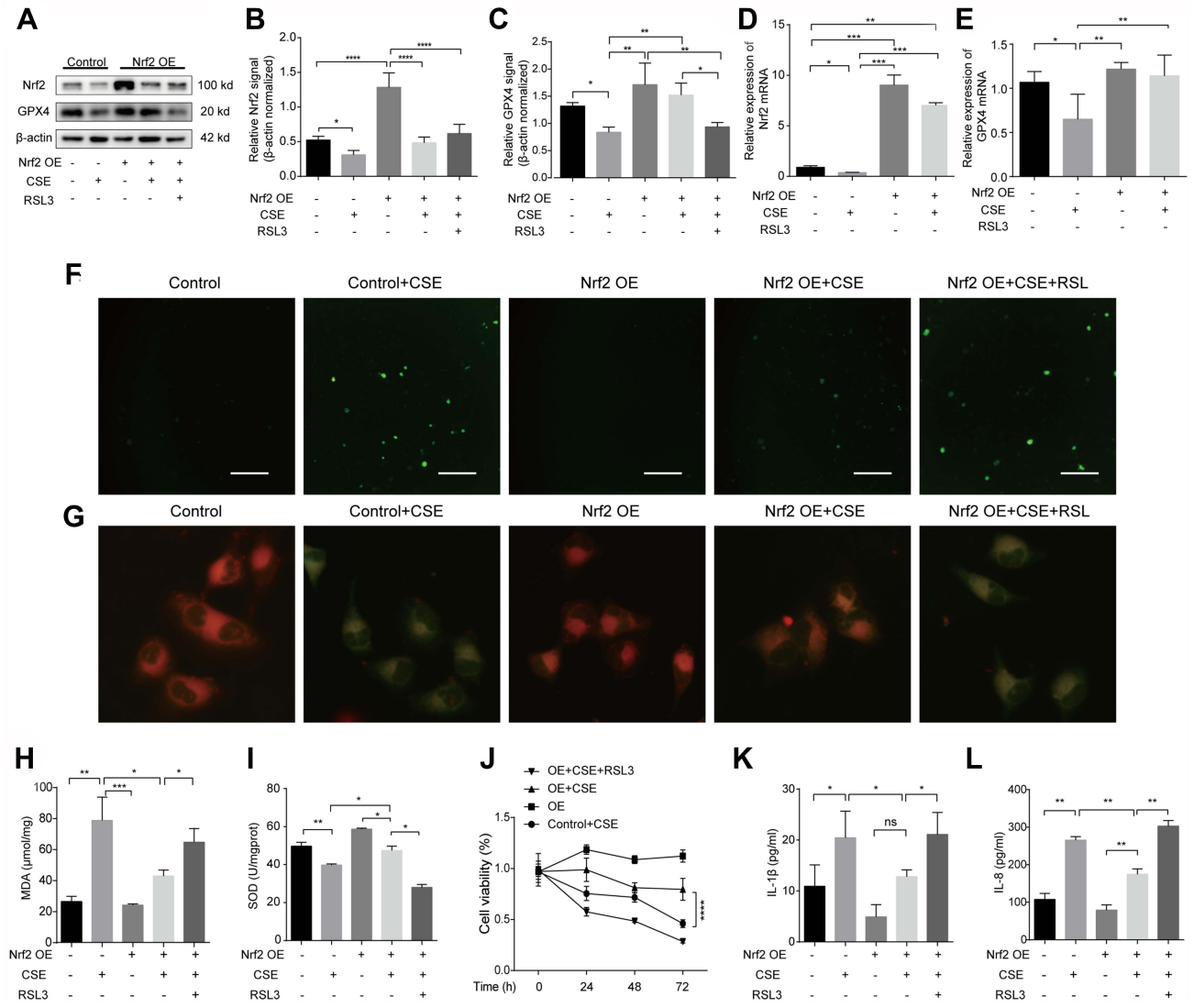

Figure 5 The Nrf2-GPX4 axis mitigates CSE-induced ferroptosis and the release of IL-1β and IL-8 in HBE cells. (**A–L**) HBE cells were transfected with Nrf2 overexpression vector (Nrf2 OE) or control vector. The OE and control groups were treated with 0% CSE or 5% CSE. Nrf2-overexpressing HBE cells were treated with 1 μmol/L RSL3 1 h before CSE exposure. (**A** and **B**) Nrf2 protein levels were detected by Western blot analysis and normalized to β-actin levels. (**A** and **C**) The protein expression of GPX4 was detected by Western blots and normalized to that of β-actin. (**D**) The mRNA level of Nrf2 was measured by RT-qPCR and normalized to that of GAPDH. (**E**) The mRNA level of GPX4 was measured by RT-qPCR and normalized to that of GAPDH. (**F**) Images of intracellular ROS stained by DCFH-DA were captured with a fluorescence microscope. Original magnification ×100. Bar: 200μm. (**G**) Representative images of C11BODIPY were captured with a fluorescence microscope in the green and red channels. An overlay of the green and red channels is shown. Original magnification ×400. (**H**) MDA and (**I**) SOD levels in each group. (**J**) Cell viability of each group was analyzed by the CCK-8 assay, and all values were normalized to those of the control group. (**K**) ELISAs of IL-1β and (**L**) IL-8 levels are shown in the supernatant of each group. The results are presented as the means ± S.E.M. for three independent experiments. *P<0.05; **P < 0.01; ***P < 0.001; ****P < 0.0001; ns: P>0.05.

Discussion

COPD is a complex polyclinic lung disease characterized by emphysema and progressive airflow obstruction. CS is the major risk factor for the pathogenesis of COPD and stimulates cellular ROS production in the lung. Lipid peroxidation and ferroptosis induced by CS participate in the process of COPD.[24] Our study indicated that CS initiated ferroptosis in bronchial epithelial cells, which could be inhibited by activation of the Nrf2/GPX4 axis. Inhibition of ferroptosis or upregulation of Nrf2/GPX4 signaling reduced IL-8 and IL-1β production, indicating a proinflammatory role in ferroptosis. Thus, CS-induced hypermethylation may result in abnormal expression of Nrf2, and targeting methylation and ferroptosis has the potential to prevent the progression of COPD.

Ferroptosis is a novel regulated cell death process that is more immunogenic due to the release of DAMPs and alarmins than apoptosis, switching the extracellular environment to a proinflammatory state.[34,36] Ferroptosis has been found to be involved in cancer, degenerative brain diseases, and

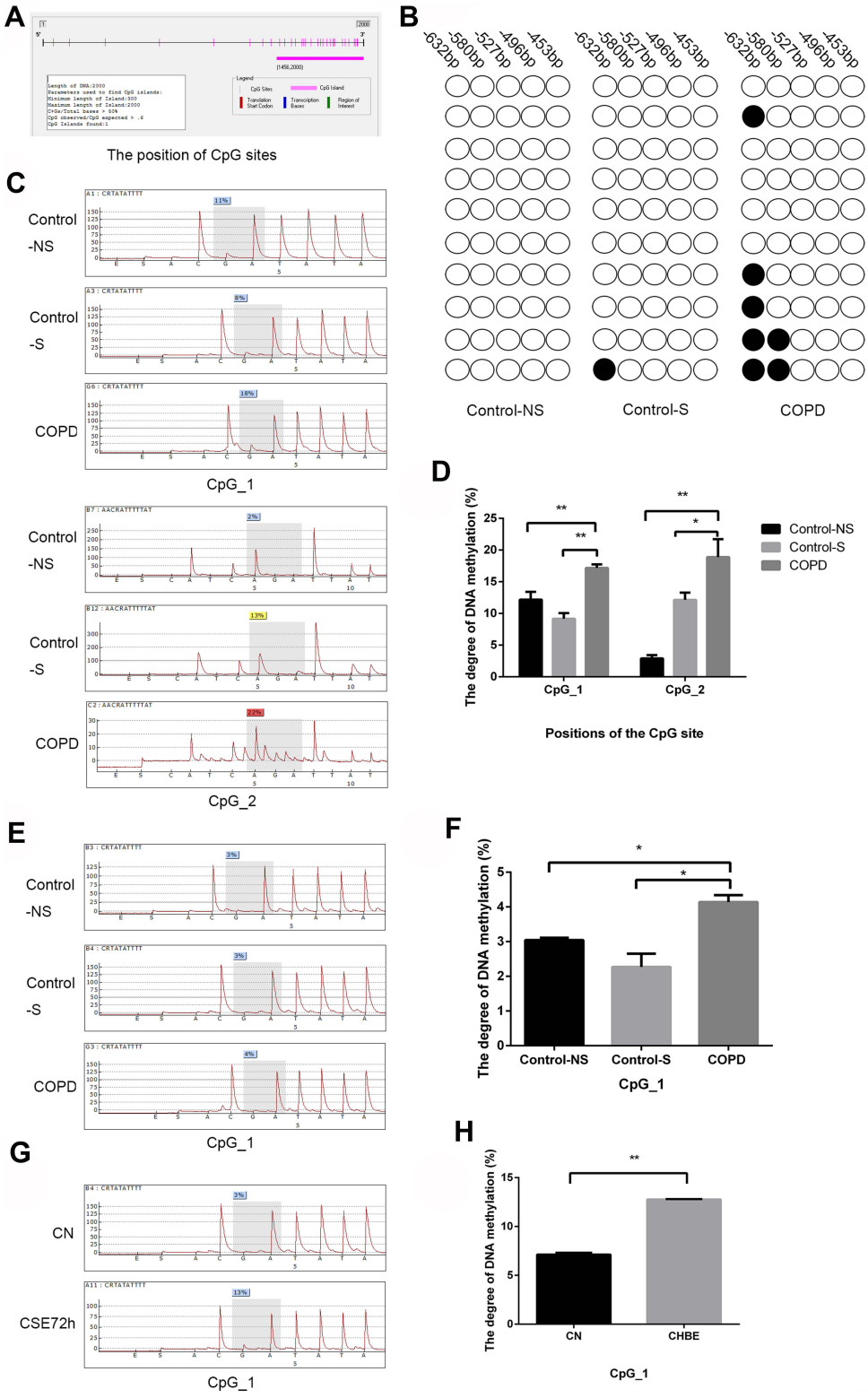

Figure 6 Specific CpG sites in the Nrf2 promoter are hypermethylated in human COPD lung and CSE-treated HBE cells. Hypermethylation of the Nrf2 promoter in COPD tissues, primary bronchial epithelial cells and HBE cells. (**A** and **B**) Bisulfite sequencing analysis (BSP) was performed to determine the CpG methylation status of the Nrf2 promoter (−632 to −1 bp) in peripheral lung tissues. Methylated (●) and unmethylated (○) CpGs are indicated. The first two CpG sites (CpG_1, −632 bp and CpG_2, −580 bp) were hypermethylated in peripheral lung tissues. (**C** and **D**) The first two sites were methylated in lung tissues from COPD patients as assessed by pyrosequencing analysis. (**E** and **F**) Only the first CpG site exhibited methylation in primary bronchial epithelial cells based on pyrosequencing analysis. (**G** and **H**) HBE cells were treated with 0% or 5% CSE for 72 h. Only the first site exhibited methylation in 5% CSE-treated HBE cells based on pyrosequencing analysis. All data are shown as means ± S.E.M. *P<0.05; **P < 0.01.

ischemia-reperfusion injuries.[35,37] In our study, we determined that ferroptosis participates in the pathogenesis of COPD, resulting in the deposition of nonheme iron and 4-HNE, an aldehyde product of phospholipid peroxidation in bronchial epithelial cells in vivo, consistent with the results of a previous study.[24] CSE induced the generation of lipid peroxidation and decreased cell viability in vitro, along with a decrease in GPX4. Moreover, CSE induced the release of IL-8 and IL-1β. The changes above could be reversed by the ferroptosis inhibitor fer-1. Ferroptosis in COPD causes the death of bronchial epithelial cells and the release of DAMPs, cytokines and ROS, leading to abnormal damage, repair and amplification of the inflammatory process and finally resulting in emphysema and airway narrowing in COPD.[24] The mechanism of ferroptosis in COPD pathogenesis is expected to be further studied. Preventing ferroptosis may be a novel target for COPD treatment.

GPX4 catalyzes the reduction of membrane lipid hydroperoxides to lipid alcohols, and this process prevents the iron-dependent formation of toxic lipid ROS using GSH as an essential cofactor.[36,38,39] Several GPX4 inhibitors, such as (1S,3R)-RSL3 (RSL3) and ML162, initiate ferroptosis.[39] In our study, GPX4 expression was significantly downregulated in primary bronchial epithelial cells of COPD patients and a murine model. CSE also induced GPX4 degradation in HBE and A549 cells. GPX4 overexpression reduced the release of DAMPs and proinflammatory cytokines from lung epithelial cells in CS-exposed mice.[24] Moreover, overexpression of GPX4 in a COPD mouse model prevented ferroptosis and the COPD phenotypes of emphysema and reduced airway thickness,[24] indicating the critical role of GPX4 in the ferroptosis and pathogenesis of COPD.

Nrf2 protects against COPD through antioxidative stress and inflammation in the lung. A previous study showed that the Nrf2 level was lowered in the lung tissues of aged smokers and COPD patients.[19,40] In the current study, we demonstrate that the Nrf2 protein is significantly decreased in the peripheral lungs of patients with COPD. Moreover, Nrf2 is located in epithelial cells in lung tissues. We also report for the first time that the expression of Nrf2 was low in primary epithelial cells derived from COPD patients. Nrf2 protein levels were negatively correlated with pulmonary oxidative injury and abnormal inflammation.

Previous studies indicated that activation of the Nrf2-GPX4 pathway enhanced the expression of a variety of antioxidants and protected cells from damage caused by ferroptosis and enhanced drug resistance.[41–43] As Nrf2 and GPX4 expression was decreased in response to CS, we sought to determine whether the Nrf2/GPX4 pathway plays a role in the inhibition of CSE-induced ferroptosis. Nrf2 overexpression reduced the level of ROS and lipid peroxidation and enhanced SOD, indicating reduced ferroptosis in response to CSE. At the same time, GPX4 expression was enhanced at the mRNA and protein levels. Upregulation of Nrf2 expression reduced the release of IL-8 and IL-1β. The protective effect could be reversed by treatment with RSL3, a small molecule that binds to and inactivates GPX4, which indicates a significant protective role of Nrf2/GPX4 in ferroptosis.

Nrf2 targets many antioxidative genes regulating ferroptosis. These targets can be divided into three broad classes: iron/metal metabolism (eg, FTH1, HO-1), intermediate metabolism (eg, G6PD, PPARG), and GSH synthesis/metabolism (eg, GPX4, SLC7A11), all of which have a verified ARE and are implicated in ferroptosis.[27] During GSH synthesis, cysteine is transported into cells via a cystine/glutamate antiporter dubbed system Xc- and then reduced to generate GSH by two enzymes, glutamate-cysteine ligase (GCL) and glutathione synthetase (GSS).[44] Nrf2 participates in GSH synthesis by the upregulating system Xc- (SLC7A11) and the rate-limiting enzymes GCL and GSS.[17,44] Enzymes that are involved in GSSG reduction or utilize GSH or NADPH to reduce oxidized substrates are also targets of Nrf2.[44] GPX4 is the main neutralizer of lipid peroxides and GSH eliminates lipid ROS via the action of GPX4. GXP4 is upregulated by Nrf2 by binding to the ARE of the GPX4 locus.[45] The details above demonstrate the role of Nrf2 in preventing the initiation of ferroptosis via GSH synthesis/metabolism and multiple pathways. As GPX4 uses GSH as an essential cofactor while catalyzing lipid hydroperoxides, exhausting GSH could inhibit the activity of GPX4,[46] indicating that GPX4 may be regulated by Nrf2 via Nrf2 binding to the ARE of the GPX4 locus or the regulation of GSH synthesis and metabolism. Considering that other Nrf2 target genes are involved in the inhibition of ferroptosis or the protection of COPD, Nrf2 pathways in ferroptosis of COPD and the complex regulatory network should be further evaluated.

It is well established that epigenetic alterations can affect gene expression.[47] Hypermethylation of CG-rich regions (CpG islands) usually inhibits gene expression, while demethylation often reactivates gene expression, thus playing a critical role in cell proliferation, differentiation and development.[48] DNA methylation frequently occurs at CpG islands, which usually have a GC content percentage of more than 50% and a CpG ratio of at least 60%.[49–51] A recent study

reported that the suppression of Nrf2 expression in the lung tissue of COPD patients was caused by CpG hypermethylation in the promoter.[52] In the current study, the first two CpG sites of the Nrf2 promoter were observed to be specifically hypermethylated in peripheral lung tissues, but only the first CpG site was hypermethylated in cultures of primary epithelial cells. One possible reason for the different hypermethylation profiles could be differences between the in vitro and in vivo environments.

Further studies may need to be conducted to elucidate the mechanism of ferroptosis in the pathogenesis of COPD. Animal models should be used to explore the role of the Nrf2/GPX4 pathway in COPD. HO-1, NQO-1 and other targets in the Nrf2 antioxidant system have been shown to be involved in ferroptosis, and these targets have been previously demonstrated to participate in COPD. The influence of the Nrf2-ARE interaction on ferroptosis and COPD needs to be further studied.

Conclusions

In summary, the current study shows that Nrf2/GPX4 activation can alleviate ferroptosis and inflammation in COPD. DNA hypermethylation at specific CpG sites of the Nrf2 promoter in primary epithelial cells and in clinical lung tissues is correlated with decreased Nrf2 expression, which is related to the occurrence and development of COPD. Further study of DNA methylation of Nrf2 and its role in regulating ferroptosis in a larger cohort is needed to validate these data.

Abbreviations

Nrf2, nuclear factor E2-related factor 2; COPD, chronic obstructive pulmonary disease; CSE, cigarette smoke extract; HBE cell, human bronchial epithelial cell; ROS, reactive oxygen species; Keap1, Kelch-like ECH-associated protein 1; ARE, antioxidant response element; GPX4, glutathione peroxidase 4; HO-1, heme oxygenase-1; NQO-1, NAD(P)H quinone oxidoreductase 1; CpG islands, CG-rich regions; DAMPs, damage-associated molecular patterns.

Data Sharing Statement

All data generated or analyzed during this study are included in this published article.

Ethics Approval and Consent to Participate

All experimental work was approved by the ethical review board of Wuxi People's Hospital Affiliated to Nanjing Medical University. This study was conducted in accordance with the Declaration of Helsinki. The procedures for the care and use of animals were approved by the Ethics Committee of Nanjing Medical University (KY21023). The animals used in this study were maintained in accordance with the ethical guidelines of the Guiding Principles in the Care and Use of Animals (China) and the Policy of Animal Care and Use Committee of Nanjing Medical University. Humane care was provided according to the 3R principles of animal experiments.

Acknowledgments

We would like to express our sincere gratitude to Peibo Li for his constructive comments.

Author Contributions

All authors made a significant contribution to the work reported, whether that is in the conception, study design, execution, acquisition of data, analysis and interpretation, or in all these areas; took part in drafting, revising or critically reviewing the article; gave final approval of the version to be published; have agreed on the journal to which the article has been submitted; and agree to be accountable for all aspects of the work.

Funding

The study was supported by the Translational Medicine Program of Wuxi City, Jiangsu Province [2020ZHYB13], the Health Department of Wuxi City, Jiangsu Province [M202032], and the Top Talent Support Program for young and middle-aged people of the Wuxi Health Committee [BJ2020006].

Disclosure

The authors declare that they have no competing interests in this work.

References

1. Leonardo F, Pauwels RA, Hurd SS. Global strategy for the diagnosis, management, and prevention of chronic obstructive pulmonary disease: GOLD executive summary updated 2003. *Am J Respir Crit Care Med*. 2007;1:104.
2. Prange R, Thiedmann M, Bhandari A, et al. A Drosophila model of cigarette smoke induced COPD identifies Nrf2 signaling as an expedient target for intervention. *Aging*. 2018;10(8):2122–2135. doi:10.18632/aging.101536
3. Tuder RM, Zhen L, Cho CY, et al. Oxidative stress and apoptosis interact and cause emphysema due to vascular endothelial growth factor receptor blockade. *Am J Respir Cell Mol Biol*. 2003;29 (1):88–97. doi:10.1165/rcmb.2002-0228OC

4. Giangreco A, Groot KR, Janes SM. Lung cancer and lung stem cells: strange bedfellows? *Am J Respir Crit Care Med*. 2007;175(6):547–553. doi:10.1164/rccm.200607-984PP
5. Hogg JC. Pathophysiology of airflow limitation in chronic obstructive pulmonary disease. *Lancet*. 2004;364(9435):709–721. doi:10.1016/S0140-6736(04)16900-6
6. de Marco R, Accordini S, Marcon A, et al. Risk factors for chronic obstructive pulmonary disease in a European cohort of young adults. *Am J Respir Crit Care Med*. 2011;183(7):891–897. doi:10.1164/rccm.201007-1125OC
7. Toledo-Pons N, Cosio BG, Velasco MD, Casanova C. Chronic obstructive pulmonary disease in non-smokers. *Arch Bronconeumol*. 2017;53(2):45–46. doi:10.1016/j.arbr.2016.11.033
8. Martinez FD. Early-life origins of chronic obstructive pulmonary disease. *N Engl J Med*. 2016;375(9):871–878. doi:10.1056/NEJMra1603287
9. Higashi T, Mai Y, Noya Y, et al. A simple and rapid method for standard preparation of gas phase extract of cigarette smoke. *PLoS One*. 2014;9(9):e107856. doi:10.1371/journal.pone.0107856
10. Linkermann A, Stockwell BR, Krautwald S, Anders HJ. Regulated cell death and inflammation: an auto-amplification loop causes organ failure. *Nat Rev Immunol*. 2014;14(11):759–767. doi:10.1038/nri3743
11. Barnes PJ. Cellular and molecular mechanisms of chronic obstructive pulmonary disease. *Clin Chest Med*. 2014;35(1):71–86. doi:10.1016/j.ccm.2013.10.004
12. Nguyen T, Sherratt PJ, Pickett CB. Regulatory mechanisms controlling gene expression mediated by the antioxidant response element. *Annu Rev Pharmacol Toxicol*. 2003;43:233–260. doi:10.1146/annurev.pharmtox.43.100901.140229
13. Kuang F, Liu J, Tang D, Kang R. Oxidative damage and antioxidant defense in ferroptosis. *Front Cell Dev Biol*. 2020;8:586578. doi:10.3389/fcell.2020.586578
14. Kobayashi M, Li L, Iwamoto N, et al. The antioxidant defense system Keap1-Nrf2 comprises a multiple sensing mechanism for responding to a wide range of chemical compounds. *Mol Cell Biol*. 2009;29(2):493–502. doi:10.1128/MCB.01080-08
15. McMahon M, Lamont DJ, Beattie KA, Hayes JD. Keap1 perceives stress via three sensors for the endogenous signaling molecules nitric oxide, zinc, and alkenals. *Proc Natl Acad Sci U S A*. 2010;107(44):18838–18843. doi:10.1073/pnas.1007387107
16. Foronjy R, D'Armiento J. The effect of cigarette smoke-derived oxidants on the inflammatory response of the lung. *Clin Appl Immunol Rev*. 2006;6(1):53–72. doi:10.1016/j.cair.2006.04.002
17. Dong H, Qiang Z, Chai D, et al. Nrf2 inhibits ferroptosis and protects against acute lung injury due to intestinal ischemia reperfusion via regulating SLC7A11 and HO-1. *Aging*. 2020;12(13):12943–12959. doi:10.18632/aging.103378
18. Boutten A, Goven D, Boczkowski J, Bonay M. Oxidative stress targets in pulmonary emphysema: focus on the Nrf2 pathway. *Expert Opin Ther Targets*. 2010;14(3):329–346. doi:10.1517/14728221003629750
19. Suzuki M, Betsuyaku T, Ito Y, et al. Down-regulated NF-E2-related factor 2 in pulmonary macrophages of aged smokers and patients with chronic obstructive pulmonary disease. *Am J Respir Cell Mol Biol*. 2008;39(6):673–682. doi:10.1165/rcmb.2007-0424OC
20. Goven D, Boutten A, Lecon-Malas V, et al. Altered Nrf2/Keap1-Bach1 equilibrium in pulmonary emphysema. *Thorax*. 2008;63(10):916–924. doi:10.1136/thx.2007.091181
21. Rangasamy T, Cho CY, Thimmulappa RK, et al. Genetic ablation of Nrf2 enhances susceptibility to cigarette smoke-induced emphysema in mice. *J Clin Invest*. 2004;114(9):1248–1259. doi:10.1172/JCI200421146
22. Dixon SJ, Lemberg KM, Lamprecht MR, et al. Ferroptosis: an iron-dependent form of nonapoptotic cell death. *Cell*. 2012;149(5):1060–1072. doi:10.1016/j.cell.2012.03.042
23. Wen Q, Liu J, Kang R, Zhou B, Tang D. The release and activity of HMGB1 in ferroptosis. *Biochem Biophys Res Commun*. 2019;510(2):278–283. doi:10.1016/j.bbrc.2019.01.090
24. Yoshida M, Minagawa S, Araya J, et al. Involvement of cigarette smoke-induced epithelial cell ferroptosis in COPD pathogenesis. *Nat Commun*. 2019;10(1):3145. doi:10.1038/s41467-019-10991-7
25. Kerins MJ, Ooi A. The Roles of NRF2 in Modulating Cellular Iron Homeostasis. *Antioxid Redox Signal*. 2018;29(17):1756–1773. doi:10.1089/ars.2017.7176
26. Anandhan A, Dodson M, Schmidlin CJ, Liu P, Zhang DD. Breakdown of an ironclad defense system: the critical role of NRF2 in mediating ferroptosis. *Cell Chem Biol*. 2020;27(4):436–447. doi:10.1016/j.chembiol.2020.03.011
27. Dodson M, Castro-Portuguez R, Zhang DD. NRF2 plays a critical role in mitigating lipid peroxidation and ferroptosis. *Redox Biol*. 2019;23:101107. doi:10.1016/j.redox.2019.101107
28. Yang Y, Di T, Zhang Z, et al. Dynamic evolution of emphysema and airway remodeling in two mouse models of COPD. *BMC Pulm Med*. 2021;21(1):134. doi:10.1186/s12890-021-01456-z
29. He S, Li L, Sun S, Zeng Z, Lu J, Xie L. A novel murine chronic obstructive pulmonary disease model and the pathogenic role of MicroRNA-21. *Front Physiol*. 2018;9:503. doi:10.3389/fphys.2018.00503
30. Lun FM, Chiu RW, Sun K, et al. Noninvasive prenatal methylomic analysis by genomewide bisulfite sequencing of maternal plasma DNA. *Clin Chem*. 2013;59(11):1583–1594. doi:10.1373/clinchem.2013.212274
31. Liu Z, Lv X, Yang B, Qin Q, Song E, Song Y. Tetrachlorobenzoquinone exposure triggers ferroptosis contributing to its neurotoxicity. *Chemosphere*. 2021;264(Pt 1):128413. doi:10.1016/j.chemosphere.2020.128413
32. Barrera G. Oxidative stress and lipid peroxidation products in cancer progression and therapy. *ISRN Oncol*. 2012;2012:137289. doi:10.5402/2012/137289
33. Miotto G, Rossetto M, Di Paolo ML, et al. Insight into the mechanism of ferroptosis inhibition by ferrostatin-1. *Redox Biol*. 2020;28:101328. doi:10.1016/j.redox.2019.101328
34. Sun Y, Chen P, Zhai B, et al. The emerging role of ferroptosis in inflammation. *Biomed Pharmacother*. 2020;127:110108. doi:10.1016/j.biopha.2020.110108
35. Shin D, Kim EH, Lee J, Roh JL. Nrf2 inhibition reverses resistance to GPX4 inhibitor-induced ferroptosis in head and neck cancer. *Free Radic Biol Med*. 2018;129:454–462. doi:10.1016/j.freeradbiomed.2018.10.426
36. Yang WS, SriRamaratnam R, Welsch ME, et al. Regulation of ferroptotic cancer cell death by GPX4. *Cell*. 2014;156(1–2):317–331. doi:10.1016/j.cell.2013.12.010
37. Ma H, Wang X, Zhang W, et al. Melatonin Suppresses Ferroptosis Induced by High Glucose via Activation of the Nrf2/HO-1 Signaling Pathway in Type 2 Diabetic Osteoporosis. *Oxid Med Cell Longev*. 2020;2020:9067610. doi:10.1155/2020/9067610
38. Tang H, Chen D, Li C, et al. Dual GSH-exhausting sorafenib loaded manganese-silica nanodrugs for inducing the ferroptosis of hepatocellular carcinoma cells. *Int J Pharm*. 2019;572:118782. doi:10.1016/j.ijpharm.2019.118782
39. Forcina GC, Dixon SJ. GPX4 at the Crossroads of Lipid Homeostasis and Ferroptosis. *Proteomics*. 2019;19(18):e1800311. doi:10.1002/pmic.201800311
40. Kammerl I. Expression of concern: decline in NRF2-regulated antioxidants in COPD lungs due to loss of its positive regulator, and heightened endoplasmic reticulum stress in the lungs of patients with COPD. *Am J Respir Crit Care Med*. 2014;190(10):1200. doi:10.1164/rccm.190101200
41. Gou Z, Su X, Hu X, et al. Melatonin improves hypoxic-ischemic brain damage through the Akt/Nrf2/Gpx4 signaling pathway. *Brain Res Bull*. 2020;163:40–48. doi:10.1016/j.brainresbull.2020.07.011

42. Ma CS, Lv QM, Zhang KR, et al. NRF2-GPX4/SOD2 axis imparts resistance to EGFR-tyrosine kinase inhibitors in non-small-cell lung cancer cells. *Acta Pharmacol Sin*. 2020. doi:10.1038/s41401-020-0443-1
43. Liu Q, Wang K. The induction of ferroptosis by impairing STAT3/Nrf2/GPx4 signaling enhances the sensitivity of osteosarcoma cells to cisplatin. *Cell Biol Int*. 2019;43(11):1245–1256. doi:10.1002/cbin.11121
44. Lu SC. Regulation of glutathione synthesis. *Mol Aspects Med*. 2009;30(1–2):42–59. doi:10.1016/j.mam.2008.05.005
45. Salazar M, Rojo AI, Velasco D, de Sagarra RM, Cuadrado A. Glycogen synthase kinase-3beta inhibits the xenobiotic and antioxidant cell response by direct phosphorylation and nuclear exclusion of the transcription factor Nrf2. *J Biol Chem*. 2006;281(21):14841–14851. doi:10.1074/jbc.M513737200
46. Abdalkader M, Lampinen R, Kanninen KM, Malm TM, Liddell JR. Targeting Nrf2 to suppress ferroptosis and mitochondrial dysfunction in neurodegeneration. *Front Neurosci*. 2018;12:466. doi:10.3389/fnins.2018.00466
47. Momparler RL. Epigenetic therapy of cancer with 5-aza-2′-deoxycytidine (decitabine). *Semin Oncol*. 2005;32(5):443–451. doi:10.1053/j.seminoncol.2005.07.008
48. Liu CM, Ma JQ, Xie WR, et al. Quercetin protects mouse liver against nickel-induced DNA methylation and inflammation associated with the Nrf2/HO-1 and p38/STAT1/NF-kappaB pathway. *Food Chem Toxicol*. 2015;82:19–26. doi:10.1016/j.fct.2015.05.001
49. Portela A, Esteller M. Epigenetic modifications and human disease. *Nat Biotechnol*. 2010;28(10):1057–1068. doi:10.1038/nbt.1685
50. Roman T, Aumüller E, Berner C, Haslberger AG. Interaction of Hereditary and Epigenetic Mechanisms in the Regulation of Gene Expression. In: *Epigenetics and Human Health*. 2009:13–34. doi:10.1002/9783527628384.ch4
51. Guerrero-Bosagna C, Valladares L. Epigenetically induced changes, and transgenerational transmission of characters and epigenetic states. *Endocrine Disruptors*. 2007; 175.
52. Vucic EA, Chari R, Thu KL, et al. DNA methylation is globally disrupted and associated with expression changes in chronic obstructive pulmonary disease small airways. *Am J Respir Cell Mol Biol*. 2014;50(5):912–922. doi:10.1165/rcmb.2013-0304OC